For the published version, please refer to P. Moras et al., Phys. Rev. B 103, 165426 (2021)
DOI: https://doi.org/10.1103/PhysRevB.103.165426

Reference plane for the electronic states in thin films on stepped surfaces

P. Moras[1*], T. O. Menteş[2], F. Schiller[3,4], L. Ferrari[5], D. Topwal[6,7], A. Locatelli[2], P. M. Sheverdyaeva[1], and C. Carbone[1]

[1]Istituto di Struttura della Materia-CNR (ISM-CNR), Trieste 34149, Italy
[2]Elettra - Sincrotrone Trieste S.C.p.A., Basovizza, Trieste 34149, Italy
[3]Centro de Fisica de Materiales CSIC/UPV-EHU-Materials Physics Center, E-20018 Donostia-San Sebastian, Spain
[4]Donostia International Physics Center, E-20018 Donostia-San Sebastian, Spain
[5]Istituto di Struttura della Materia-CNR (ISM-CNR), Roma 00100, Italy
[6]Institute of Physics, Sachivalaya Marg, Bhubaneswar 751005, India
[7]Homi Bhabha National Institute, Training School Complex, Anushakti Nagar, Mumbai 400094, India

(Dated: March 04, 2021)

[*]Corresponding author: paolo.moras@trieste.ism.cnr.it

The question on whether there exists a unique photoelectron reference plane for a stepped solid surface is discussed on the basis of angle-resolved photoelectron spectroscopy data for Ag films grown on Pt(997). Different step morphologies at the surface and interface, revealed by low-energy electron diffraction measurements, result in distinctly different band dispersions of the *sp*-like quantum well states and of the Shockley surface state. Quantum well standing waves form between the parallel optical surface and interface planes, while the surface state follows the orientation of a local plane tilted with respect to the optical surface. These findings show the connection of the photoelectron reference plane with the local morphology of a solid surface and the spatial extent of the electron wave functions.

I. INTRODUCTION

The description of the surface electronic structure of a crystalline solid may depend on the lateral length scale, which is especially evident in the case of stepped surfaces. A consequence is seen in the photoelectric effect, in which an electron is emitted from the surface into the vacuum. The discrete translational symmetry of crystalline surfaces imposes that, during the photoemission process, the parallel component of the photoelectron momentum $\vec{k}_{\parallel}$ is conserved across the modulation plane of the wave function, i.e. the so-called reference plane [1]. The identification of this plane is straightforward for low Miller index surfaces, where the average (optical) surface and the terrace plane coincide. On the other hand, the choice of a reference plane becomes questionable for surfaces of lower symmetry.

Detailed experimental analysis on this point has been carried out by angle-resolved photoelectron spectroscopy (ARPES) using noble metal crystals vicinal to (111), which present periodic step-terrace structures and parabolic-like Shockley surface states near the Fermi level (E_F) [2]. For narrow terraces the surface electrons are weakly affected by the steps, propagate along the average surface as coherent two-dimensional (2D) super-lattice states and replicate at $k_{\parallel,n} = (2n-1)\pi/d$, where $n \geq 1$ is an integer number and d the periodic inter-step distance. For larger terraces the steps tend to confine the surface electrons within the terrace width and to form discrete quasi one-dimensional (1D) energy levels. The reference planes for the 2D and 1D states are the optical surface and the terrace plane, respectively. The origin of the transition from the 2D to the 1D band behavior has been thoroughly debated [3-16]. Recent investigations suggest that the effects of 1D confinement derive from the reduced structural order of the step lattice for large inter-step distances [17]. The ARPES analysis of faceted crystals [18] and Ag stripes on Cu vicinal surfaces [1,19,20] shows in a direct way how the local surface atomic structure, rather than the optical surface, defines the photoelectron reference plane in nano-structured systems.

All the studies cited above deal with surface electronic features, while the behavior of the bulk states in the same kind of systems has received little attention. In the present paper we will examine experimentally the concept of photoelectron reference plane for the surface and "bulk-like" electronic states of thin films grown on a regularly stepped substrate. Similar studies have been carried out by ARPES for a couple of cases [21,22]. Ag films on various surfaces vicinal to Au(111) present the same step-terrace morphology of the substrates, thanks to the optimal Ag/Au lattice matching [21]. The optical surface and interface planes act as parallel potential walls for the *sp* valence electrons of the films, thus leading to the formation of discrete "bulk-like" quantum well (QW) states, in close analogy with thin films grown on low Miller index surfaces. The film surface plays the role of

reference plane for both Shockley surface state and QW states, which propagate as 2D super-lattice states and replicate with the same periodicity $k_{\parallel,n} = (2n-1)\pi/d$ in the reciprocal space. Ag films on Au-stabilized Si(557) show similar properties [22].

Our ARPES data for thin Ag(111)-like films on Pt(997) highlight a more complex scenario. The *sp*-derived QW states and the Shockley surface state behave as 2D electronic features with distinct reference plane and periodicity. This observation is substantiated by low-energy electron diffraction (LEED) analysis. The lattice mismatch between face centered cubic Ag and Pt (~4%) leads to the formation of nano-structured Ag films. Their surface presents an ordered sequence of terraces and double atomic steps, in registry with the step-terrace structure of Pt(997), which keeps the film thickness uniform. The QW standing waves extend within the whole film thickness and bounce between the parallel interface and surface optical planes. The photoemission pattern of the surface-localized state is determined by the orientation of a tilted plane defined by the local step-terrace structure. We conclude that two photoelectron reference planes coexist in our system due to the nano-structured morphology of the surface (different from the stepped substrate) and the characteristic spatial localization (surface vs "bulk-like") of the electronic states.

The paper is organized as follows. Section III reports ARPES data for Ag films on Pt(997). Section IV describes the kinematic model used to interpret the LEED data from stepped surfaces and its application to the cases of Pt(997) and Ag/Pt(997). Section V discusses the ARPES results in light of the structural model derived from the LEED analysis.

II. EXPERIMENTAL

Platinum stepped surfaces close to the (111) surface are characterized by highly ordered arrays of (111) terraces separated by single atomic steps caused by elastic and entropic step interaction [23]. X-ray diffraction analysis shows quantitatively the pronounced repulsive step-step interactions in Pt(997) [24]. In this system the (111) terraces are separated by periodically distributed and single-atom high steps running parallel to the $[1\bar{1}0]$ direction (in the following the x and y axes are defined as the directions perpendicular and parallel to the steps on the Pt(997) surface, respectively). The terraces consist of 8.33 atomic rows, corresponding to a terrace width L_{Pt} = 20.02 Å, a vicinal angle α_{Pt} = 6.46°, and an inter-step distance $d_{Pt} = L_{Pt}/\cos \alpha_{Pt}$ = 20.15 Å.

The Pt(997) surface has been prepared by Ar ion sputtering (2×10^{-5} mbar Ar, 1.2 keV), annealing at 870 K in molecular oxygen (5×10^{-8} mbar O_2) and flashing to 1000 K in the 10^{-10} mbar pressure range. A slow cooling rate (about 1 K/sec) has been employed to stabilize a regular step-terrace surface morphology [25]. As shown in Fig. 1(a), already after few cycles of sputtering and

annealing the LEED pattern visualizes energy-dependent coexisting spots along the x-axis and very low intensity between the spots indicating a highly ordered surface. The substrate has been kept at about 150 K during Ag deposition (2 Å per minute) and warmed-up to room temperature. This "two-step" growth procedure has been used on several low-index [26] and quasicrystalline [27] surfaces and turns out to be suitable to produce uniform Ag films showing QW states in the ARPES spectra (see Sec. III). The film thickness is expressed in monolayers, where 1 ML = 2.36 Å corresponds to the distance between (111) planes in bulk Ag. The hexagonal LEED patterns of the Ag films display again energy-dependent coexisting spots along x and some intensity between the spots. This indicates the persistence of the step-terrace morphology along with a broader width distribution of the (111) terraces with respect to clean Pt(997). In order to directly compare the structural parameters of Ag film and substrate, a 9 ML Ag film has been grown on the substrate partially masked by a shutter. The pattern of Fig. 1(b) has been acquired with a conventional LEED apparatus (spot size ~1 mm diameter) across the sharp edge between clean and Ag-covered Pt(997). The known Pt lattice constant (3.92 Å) gives the distance between the rows of Pt spots $K_{Pt} = 2.27$ Å^{-1}, which is used to determine the distance between the rows of Ag spots $K_{Ag} = (2.19 \pm 0.03)$ Å^{-1} (the error originates from the finite spot size). This value is very close to the ideal value for the Ag(111) surface 2.17 Å^{-1}, thus revealing that the 9 ML film is fully relaxed along the y axis. This observation is valid in the whole investigated range of Ag film thickness (9÷22 ML).

Photoemission experiments have been performed at the VUV-Photoemission Beamline (Elettra, Trieste). ARPES spectra have been measured at room temperature, using a Scienta R-4000 electron analyzer and photon energies ($\hbar\omega$) between 19.7 and 171 eV. Energy and angular resolutions have been set to 25 meV and 0.3°. The Pt[997] axis (normal emission direction) corresponds to $\vec{k}_{\parallel} = (k_x, k_y) = (0,0)$.

The LEED measurements have been carried out using the Spectroscopic PhotoEmission and Low-Energy Electron Microscope (SPELEEM) installed at the Nanospectroscopy Beamline (Elettra, Trieste) [28,29]. The instrument can be operated either as an x-ray or electron microscope [30]. The latter modality is based on the elastic back-scattering of low-energy electrons. LEED data can be collected by imaging the back-focal plane of the objective lens. The LEED pattern originates from a micron-sized region determined by an aperture that defines the focused incident beam size. The transfer width of the instrument is about 130 Å together with 0.5 eV energy spread of the LaB_6 source [29]. Due to the constant electron kinetic energy in the imaging column (independent of the electron energy incident on the surface) the LEED spots remain at constant position at the back-focal plane for varying incident electron energy. Therefore, the parallel momentum transfer $\vec{q}_{\parallel}$ in the diffraction pattern can be easily calibrated regardless of the electron energy. The calibration of the q-space has

been done independently using the LEED spot separations from a clean Re(0001) crystal. The systematic errors in the calibration due to different sample alignments and due to anisotropic distortions are estimated to be below a few percent.

III. ARPES ANALYSIS

The electronic structure of the Ag/Pt(997) system in the sub-ML and few ML regime has been analyzed previously by valence band photoelectron spectroscopy [31] and two-photon ARPES [32,33]. The present paper focuses on larger Ag thicknesses, that allow the formation of continuous films and the observation of QW states. Fig. 2 reports ARPES data for an 18 ML Ag film. Fig. 2(a) shows a selection of spectra taken at different photon energies along the x axis. The k_x coordinate is determined through the equation:

$$k_x = \sqrt{\frac{2m_e}{\hbar^2}(\hbar\omega - \Phi - E_B)}\sin\theta_x \qquad (1)$$

where m_e is the electron mass, Φ the sample work function, E_B the binding energy, and θ_x the emission angle with respect to the normal photoelectron emission direction. The energy scale is referred to E_F. Besides intensity variations due to matrix element effects, all panels reveal the presence of the Shockley surface state near E_F (arrows) and two *sp*-derived QW states (dashed lines) with parabolic-like dispersion. The formation of QW states in thin metal films is associated with the presence of a confining potential barrier at the interface. Film states that cannot hybridize to substrate states with compatible symmetry become confined within the film and give rise to discrete QW bands, in analogy to the particle-in-a-box picture [26]. The flattening of the QW band bottom in our ARPES data is ascribed to the hybridization between Ag and Pt bands with common Λ_1 symmetry, as previously discussed for Ag films on Pt(111) [34]. ARPES studies of thin metal films demonstrate the sensitivity of the QW states to thickness variations as small as 1 ML [21,26]. The observation of well-defined peaks in Fig. 2 is a direct evidence of the uniform thickness of the Ag film on Pt(997).

The QW states disperse symmetrically about non-zero $k_{x,n}$ values, which remain constant within the experimental error (0.015 $Å^{-1}$) for extended photon energy ranges, called “zones” in the nomenclature of Ref. [22]. This behavior is best visualized in Fig. 2(c) that shows the positions of the QW band center (full squares) as a function of the photon energy in the (k_x,k_z) plane (structure plot). The k_z position of the QW band center is determined through the equation:

$$k_z = \sqrt{\frac{2m_e}{\hbar^2}\left[(\hbar\omega - \Phi - E_B)\cos^2\theta_x - V_0\right]} \quad (2)$$

where the inner potential V_0 is set to -11.5 eV, as for Ag(111) [35]. Linear fittings to the three rods of data give: $k_{x,1}$ = 0.11 Å^{-1}; $k_{x,2}$ = 0.33 Å^{-1}; $k_{x,3}$ = 0.55 Å^{-1}. These values can be described by the formula $k_{x,n} = k_{QW}(2n-1)/2$, i.e. the QW states replicate with period k_{QW} = (0.22±0.015) Å^{-1} in the reciprocal space. As for the LEED pattern of Fig. 1 (see also Sec. IV), the scattering potential giving origin to the QW state replicas is attributed to the presence of a stepped surface, whose periodicity in the real space is obtained as $d_{Ag} = 2\pi/k_{QW}$ = (28.6±2.0) Å, which is significantly larger than d_{Pt} = 20.15 Å.

The surface state is visible near the $k_{x,n}$ values in Fig. 2(a) (white arrows). At variance with the QW states, the position of the surface state changes along k_x within each "zone". For instance, Fig. 2(b) highlights by the green continuous line the crossing of $k_{x,2}$ when increasing the photon energy. These spectra have been normalized to the Fermi function in order to visualize the surface state up to 120 meV above E_F [36]. The observation of the expected parabolic dispersion (green dashed line) excludes the interference of other spectral features, like surface and/or QW state replicas, or the hybridization with the Pt states [34] in the k_x shift. The energy position of the surface state band bottom at ~20 meV is determined by the combination of thermal effects [37] and depopulation induced by the finite size of the terrace width [38,39].

The position of the surface state band center is represented by full circles in Fig. 2(c). For these data the experimental error is increased to ±0.02 Å^{-1}, due to the limited k_x range available for the parabolic fitting. The surface state data lie on three equally-spaced rods (dashed lines) forming an angle β_{Ag} = (2.25±0.25) ° with the Pt[997] direction (k_z axis). This behavior has not been reported in previous studies of Ag films on stepped surfaces [21,22] and differs from the dispersion of the surface state in vicinal surfaces with large inter-step distances [17].

In order to determine the separation between the three rods (k_{SS}), we apply the so-called direct rotation correction [1]. This procedure is based on the fact that the surface state is a 2D electronic feature, whose k_x dispersion must not depend on k_z. Practically, it consists in the rotation of the k_x and k_z axes by an angle (β_{Ag}) that makes the surface state rods vertical, i.e. non-dispersive as a function of the photon energy (Fig. 2(d)). We obtain k_{SS} = (0.11±0.02) Å^{-1} ≈ $k_{QW}/2$. The structural element associated to k_{SS} and the relation between k_{SS} and k_{QW} will be clarified in Sec. V on the basis of the LEED analysis.

The experimental observations reported above do not depend on the specific film thickness within a wide thickness range (9÷22 ML). Fig. 3 shows ARPES data of a 12 ML Ag film on Pt(997). Also in this case surface and QW states behave differently, as can be seen in the photon energy

dependent ARPES spectra (panel (a)) and in the structure plot (panel (b)). The k_{SS} and k_{QW} values for the 12 ML film are very close to those observed for the 18 ML film.

Fig. 3(c) reveals another notable feature of the Ag films on Pt(997). The shape of the surface and QW state contours in the constant energy cut at 80 meV above E_F (top of Fig. 3(c)) appears to be elongated in the k_x direction, in contrast with the isotropic character of *sp*-like electronic states in Ag(111) films near the center of the surface Brillouin zone. The elliptical shape derives from the fact that the band aperture along k_x is about 33% bigger than along k_y (bottom of Fig. 3(c)). These data recall the electronic states of Ag films grown on In/Si(111) [40,41] and GaAs(110) [42], which display 1D structural modulations. In those systems the anisotropic band dispersion has been ascribed to the presence of densely distributed stacking fault planes crossing the entire film thickness, which act as finite potential walls for the electron propagation along one in-plane direction. In Ag films on Pt(997) the formation of stacking fault planes could be favored by the step-terrace morphology of the substrate and the difference between the lattice parameters of Ag and Pt.

Overall, the experimental data of Figs. 2 and 3 show that the Ag film thickness is uniform and the QW state dispersion refers to the parallel surface and interface planes. The surface state behavior, instead, indicates the presence of a second reference plane tilted off the average surface towards the Pt[111] axis by the angle β_{Ag}. Surface and QW states replicate periodically in the reciprocal space with different, but related, periods k_{SS} and k_{QW}. This scenario clearly departs from previous findings for Ag(111) films grown on vicinal surfaces [21,22].

IV. LEED ANALYSIS

The structural properties of Ag films on Pt(997) can be determined by LEED analysis. The main aspects of LEED from stepped surfaces have been established several decades ago [43,44]. Experiments demonstrate that the LEED pattern of stepped surfaces typically shows split spots [45], as seen in Fig. 1. By analyzing the energy dependence of the specular beam position in the reciprocal q-space it is possible to extract the changes in the average terrace width and surface orientation of the Ag films with respect to the clean substrate. The analytical frame needed to describe LEED from stepped surfaces is recalled below.

A. LEED from stepped surfaces

Fig. 4(a) shows a side-view sketch of a stepped surface oriented at an arbitrary angle with respect to the incidence direction of the electron beam. Assuming perfectly ordered straight steps, the

system can be described by the terrace width (L), the angle between the terraces and the optical surface (α) and the angle between the normal to the optical surface and the direction of the incident beam (β). The surface is partitioned into repeating units $s(\vec{r})$, which are obtained by slicing the crystal along the incidence direction at each surface step. The coordinate system is aligned according to the incident beam, with the z axis along the incidence direction and the x axis aligned perpendicularly to the step direction ($\vec{r}$ = (x,z)). Notably, L is univocally determined by α, if the lattice constant of the crystal is known.

The scattering amplitude is a sum over the real space structure with phases equal to the product of the momentum transfer and the atomic positions, which can be written as:

$$F(\vec{q}) = \int f(\vec{r}) e^{i\vec{q}\cdot\vec{r}} d\vec{r} \quad (3)$$

where $\vec{q}=\vec{k}_f-\vec{k}_i$ is the momentum transfer between initial and final state, and $f(\vec{r})$ is the crystal lattice. With the partitioning sketched in Fig. 4, the lattice can be expressed as the sum:

$$f(\vec{r}) = \sum_m s(\vec{r}-m\vec{r}_0) \quad (4)$$

where $\vec{r}_0$ is the vector separating two consecutive steps on the surface and m is an integer. With this partitioned lattice the scattering amplitude becomes:

$$F(\vec{q}) = \sum_m \int s(\vec{r}-m\vec{r}_0) e^{i\vec{q}\cdot\vec{r}} d\vec{r} = \left(\sum_m e^{im\vec{q}\cdot\vec{r}_0}\right)\left(\int s(\vec{r}) e^{i\vec{q}\cdot\vec{r}} d\vec{r}\right) \quad (5)$$

The second term in the final product is the structure factor, $S(\vec{q})$, corresponding to the Fourier transform of a single repeating unit $s(\vec{r})$. The first term produces the diffraction from the superstructure. The infinite summation results in periodic delta-functions located at positions corresponding to the condition $\vec{q}\cdot\vec{r}_0 = 2\pi m$. According to the sketch in Fig. 4, the vector $\vec{r}_0$ can be expressed as:

$$\vec{r}_0 = \frac{L\cos\beta}{\cos\alpha}\hat{x} - \frac{L\sin\beta}{\cos\alpha}\hat{z} \quad (6)$$

Using this vector in the delta functions $\delta(\vec{q}\cdot\vec{r}_0-2\pi m)$, the scattering amplitude becomes:

$$F(\vec{q}) \propto S(\vec{q}) \sum_m \delta\left(q_x - q_z\tan\beta - \frac{2\pi m\cos\alpha}{L\cos\beta}\right) \quad (7)$$

where q_x and q_z are the components of $\vec{q}$ along the x and z axes.

This expression describes qualitatively the intensity distribution of the specular beam in the reciprocal space. It is a product of the structure factor of a single terrace with a series of lines in the q_x-q_z plane. As an example pertinent to the present paper, Fig. 4(b) shows the simulated diffraction intensity plot for the specular beam of the Pt(997) surface. The equispaced rods with angle β and separation $Q = 2\pi\cos\alpha/(L\cos\beta)$ mark the position of the delta functions in Eq. 7. The intensity maxima trace out the structure factor of the single terrace, which is inclined with respect to the incidence axis by an angle α + β. It must be underlined here that the intensity distribution in actual data is more complex due to multiple scattering effects.

Importantly, L, α and β can be obtained by analyzing the properties of the specular beam in the q_x-q_z plane. Based on these results, LEED I(V) data for clean and Ag-covered Pt(997) will be used to determine their structural parameters in the following sub-sections.

B. Pt(997) substrate

Fig. 5 reports the energy dependent intensities of the specular beam for the clean Pt(997) surface in the q_x-q_z plane. These data have been collected along the dashed line marked in Fig. 1(a) for 10÷200 eV primary electron energies. In the SPELEEM instrument the normal to the average optical surface of Pt(997) has been aligned with the incident electron beam. This experimental geometry corresponds to β = 0 °. In the present dataset the finite precision of the geometrical alignment gives rise to a small angle β_{Pt} = (0.07±0.37) °. The maxima of the LEED intensity profiles (red dots) clearly define a series of equally spaced rods separated by Q_{Pt} = (0.32±0.01) $Å^{-1}$. These rods are projections of the bulk Γ points of Pt (Γ_{Pt}), which lie along the Pt[111] axis, with the Γ_{Pt} - Γ_{Pt} distance equal to 2.78 Å. From these structural parameters it is easy to derive $\alpha_{Pt} + \beta_{Pt}$ = (6.61±0.37) °, α_{Pt} = (6.54±0.37) °, L_{Pt} = (19.51±0.63) Å, which are very close to the nominal values for Pt(997).

C. Ag films on Pt(997)

Thin Ag films on Pt(997) have been investigated with the SPELEEM instrument using the same alignment of the clean substrate. As already said with reference to Fig. 1(b), the Ag films display a hexagonal LEED pattern and spot splittings similar to those of the substrate. It is reasonable to assume that the prevalent surface morphology of the films consists of (111)-oriented terraces separated by

steps running along y. Indeed, this step-terrace morphology is stable at room temperature for Ag surfaces vicinal to (111), thanks to the contribution of the vibrational entropy at the steps [46].

Fig. 6 display energy-dependent LEED-I(V) data for the (0,0) spot of (a) 9 and (b) 15 ML Ag films on Pt(997). The maxima of every spectrum (green dots) have been overlaid to the intensity plot. The tilted slope of the diffraction spots in the q_x-q_z plane, which is highlighted by the dashed lines, is the signature of a change in the orientation of the surface termination with respect to the Pt(997) case. Linear fittings through the diffraction rods are used to derive the angle β_{Ag} (with an error of ±0.25 °) and the spot separation Q_{Ag} (with an error of ±0.015 $Å^{-1}$) for the two films. In order to determine $\alpha_{Ag}+\beta_{Ag}$, we have used the position of the diffraction spot located at q_z = 10.8 $Å^{-1}$, as it is marginally affected by multiple scattering events occurring at lower energies (i.e. at lower q_z). We estimate the error of this procedure to be ±0.4 °. Notably, the red line defining the angle $\alpha_{Ag}+\beta_{Ag}$ intercepts periodically the diffraction rods. The crossing points, indicated by red diamonds, are separated by the mean experimental distance 2.73±0.15$Å^{-1}$. This value corresponds closely to the distance between consecutive Γ_{Ag} points along the direction perpendicular to the (111) planes in bulk Ag (2.66 $Å^{-1}$). Therefore, the red line is identified with the Ag[111] axis, i.e. the direction perpendicular to the Ag(111) terraces. L_{Ag} is derived from Q_{Ag}, α_{Ag} and β_{Ag}.

The structural parameters of the two Ag films are very similar (Table I), thus indicating the formation of a stable film morphology, which persists upon changing the film thickness. The Ag surface shows a prevalent orientation characterized by the angle β_{Ag}. As the films display also a uniform thickness, this means that the surface is locally organized in step-terrace structures of finite lateral size, which are tilted by the angle β_{Ag} with respect to the Pt(997) surface. The mean width of the Ag(111) terraces is L_{Ag}. The thickness variation associated to the presence of larger terraces with respect to Pt(997) must be compensated by “local defects”, such as step bunches. The angle $\alpha_{Ag}+\beta_{Ag}$ is larger than α_{Pt} thus implying that the Ag(111) terraces are not exactly parallel to the (111) terraces of the substrate.

V. DISCUSSION

Fig. 7(a) shows the structural model for a Ag film on Pt(997) that can explain the ARPES and LEED observations reported above. It is based on the truncation of bulk Ag, without relaxation of the surface atoms. The structural details of the interface are neglected. The model presents (111) terraces parallel to those of the substrate (this point will be further discussed in the following). Every terrace consists of 11.33 atomic rows, corresponding to L_{Ag} = 28.33 Å. Two adjacent terraces are separated by a single-atom-high and [111]-oriented step, thus defining locally the (11,11,9) plane. The angle

α_{Ag} = 4.76 ° and the inter-step distance d_{Ag} = 28.35 Å are easily derived. Adjacent two-terrace structures are separated by a double atomic step, which has very low formation energy on the Ag(111) surface [47]. This double step is the simplest structural element that can fully compensate the thickness variation associated to the tilt angle β_{Ag} = 1.97 ° between the (11,11,9) plane and the optical surface. The whole Ag film can be constructed by repeating periodically the two-terrace plus double step structure. All structural parameters of the model are reported in the bottom line of Table I.

Our proposed model turns out to be particularly stable thanks to the good matching between the step-terrace structure of the substrate and the faceted structure of the film. The two continuous lines connecting the ending atoms of the Ag and Pt terraces in Fig. 7(a) highlight this matching. If measured on a (111) plane, the total width of three consecutive Pt terraces (24 Pt atomic rows) is 57.6 Å and the total width of the two-terrace plus double step structure (23 Ag atomic rows) is 57.5 Å. This corresponds to a very small tensile strain for the Ag film (~0.2 %).

The properties of the QW states are determined by the optical surface and interface planes, which are kept parallel by the two-terrace plus double step structure of the surface. The periodicity of the QW states is connected in a direct way to the size of the Ag terraces. The Shockley surface states, instead, follows the orientation of the tilted (11,11,9) plane, since its wave function is localized in the topmost atomic layers. In the (11,11,9) plane the periodicity is defined by the presence of the two terraces separated by double steps.. This explains the relation between the surface and QW state periodicity in the reciprocal space observed by ARPES ($k_{SS} \approx k_{QW}/2$).

All numerical values for the structural parameters of the model are very close to those determined by ARPES and LEED, except β_{Ag}. This difference can be explained by looking at Fig. 7(b,c), which depict the initial growth stages of Ag films on Pt(997). Ag atoms landing onto the substrate decorate the Pt steps and form pseudomorphic 1D-like island with increasing the Ag coverage (Fig. 7(b)) [48]. Due to the Ag/Pt lattice mismatch, the Ag(111) terraces of the first layer are slightly higher (in the order of 4% of the separation between (111) planes in bulk Ag, i.e. 0.094 Å) than the neighboring Pt(111) terraces. This misalignment can turn into a small tilt of the (111) terraces for the subsequent Ag layers (Fig. 7(c)). This angle sums up to β_{Ag}, while leaving α_{Ag} unaffected.

Finally, we observe that the actual structure of the Ag films can deviate from the model of Fig. 7(a) in different ways. The anisotropic dispersion of the surface and QW states of Fig. 3(c) has been ascribed to the presence of stacking fault planes crossing the entire film thickness. We suggest that these planes originate at the interface in correspondence with the structural “defects” described in Fig. 7(c). Moreover, it is clear that the high degree of structural perfection of the Pt(997) crystal drives the growth of well-ordered Ag films. However, the step-step interactions that stabilize the surface

super-structure tend to fade with increasing the Ag film thickness. Therefore, the measured Ag terrace width and periodicity of the double steps must be considered as average values of a distribution considerably broader in comparison to the terrace-width distribution of the Pt substrate. This fact can explain why the periodicity associated to the double steps is not observed in the LEED pattern.

VI. CONCLUSIONS

Thin nano-structured Ag films on Pt(997) present a more complex electronic structure with respect to previously examined films on vicinal substrates. The formation of a periodic two-terrace plus double step structure results in qualitatively different properties of the surface and QW states. The “bulk-like” character of the QW states prevails over the structural details of the surface, which is seen as a confining potential wall parallel to the interface plane. The surface state follows the orientation of the tilted (11,11,9) plane, owing to its surface-localized character. The most straightforward interpretation of these experimental observations is that two distinct photoelectron reference planes coexist in our system. In conclusion, the knowledge of the local morphology and spatial properties of the electronic states is necessary to define the photoelectron reference plane of a solid surface.

Acknowledgments

This work has been partially funded through the project EUROFEL-ROADMAP ESFRI and by the Spanish Ministry of Science and Innovation (MAT-2017-88374-P) and the Basque Government (Grant IT-1255-19).

References

[1] J. Lobo-Checa, A. Mugarza, J. E. Ortega, and E. G. Michel, New J. Phys. **13**, 103013 (2011).

[2] J. E. Ortega, A. Mugarza, F. Schiller, J. Lobo-Checa, M. Corso, Electronic States of Vicinal Surfaces. In: M. Rocca. T. S. Rahman, L. Vattuone (eds) Springer Handbook of Surface Science. Springer Handbooks. Springer, Cham. (2020)

[3] J. E. Ortega, S. Speller, A. Bachmann, A. Mascaraque, E. G. Michel, A. Närmann, A. Mugarza, A. Rubio, and F. Himpsel, Phys. Rev. Lett. **84**, 6110 (2000).

[4] F. Baumberger, T. Greber, and J. Osterwalder, Phys. Rev. B **64**, 195411 (2001).

[5] X. J. Shen, H. Kwak, D. Mocuta, A. M. Radojevic, S. Smadici, and R. M. Osgood, Phys. Rev. B **63**, 165403 (2001).

[6] J. E. Ortega, A. Mugarza, A. Närmann, A. Rubio, S. Speller, A. R. Bachmann, J. Lobo, E. G. Michel, and F. J. Himpsel, Surf. Sci. **482–485**, 764 (2001).

[7] A. Mugarza, A. Mascaraque, V. Pérez-Dieste, V. Repain, S. Rousset, F. J. García de Abajo, and J. E. Ortega, Phys. Rev. Lett. **87**, 107601 (2001).

[8] A. Mugarza, A. Mascaraque, V. Repain, S. Rousset, K. N. Altmann, F. J. Himpsel, Yu. M. Koroteev, E. V. Chulkov, F. J. García de Abajo, and J. E. Ortega, Phys. Rev. B **66**, 245419 (2002).

[9] J. E. Ortega, A. Mugarza, V. Repain, S. Rousset, V. Pérez-Dieste, and A. Mascaraque, Phys. Rev. B **65**, 165413 (2002).

[10] F. Baumberger, M. Hengsberger, M. Muntwiler, M. Shi, J. Krempasky, L. Patthey, J. Osterwalder, and T. Greber, Phys. Rev. Lett. **92**, 016803 (2004).

[11] F. Baumberger, M. Hengsberger, M. Muntwiler, M. Shi, J. Krempasky, L. Patthey, J. Osterwalder, and T. Greber, Phys. Rev. Lett. **92**, 196805 (2004).

[12] J. E. Ortega, M. Ruiz-Osés, and J. KuntzePhys. Rev. B **72**, 195416 (2005).

[13] C. Didiot, Y. Fagot-Revurat, S. Pons, B. Kierren, C. Chatelain, and D. Malterre, Phys. Rev. B **74**, 081404(R) (2006).

[14] J. Lobo-Checa, F. Meier, J. Dil, T. Okuda, M. Corso, V. Petrov, M. Hengsberger, L. Patthey, and J. Osterwalder, Phys. Rev. Lett. **104**, 187602 (2010).

[15] J. E. Ortega, M. Corso, Z. M. Abd-el-Fattah, E. A. Goiri, and F. Schiller, Phys. Rev. B **83**, 085411 (2011).

[16] N. Zaki, K. Knox, P. D. Johnson, J. Fujii, I. Vobornik, G. Panaccione, and R. M. Osgood, Phys. Rev. B **83**, 205420 (2011).

[17] J. E. Ortega, J. Lobo-Checa, G. Peschel, S. Schirone, Z. M. Abd El-Fattah, M. Matena, F. Schiller, P. Borghetti, P. Gambardella, and A. Mugarza, Phys. Rev. B **87**, 115425 (2013).

[18] M. Corso, F. Schiller, L. Fernández, J. Cordón, and J. E. Ortega, J. Phys.: Condens. Matter **21**, 353001 (2009).

[19] J. Lobo, E. Michel, A. Bachmann, S. Speller, J. Kuntze, and J. Ortega, Phys. Rev. Lett. **93**, 137602 (2004).

[20] F. Schiller, M. Ruiz-Osés, J. Cordón, and J. E. Ortega, Phys. Rev. Lett. **95**, 066805 (2005).

[21] F. Schiller, Z. M. Abd El-Fattah, S. Schirone, J. Lobo-Checa, M. Urdanpilleta, M. Ruiz-Osés, J. Cordón, M. Corso, D. Sànchez-Portal, A. Mugarza, and J. E. Ortega New J. Phys. **16**, 123025 (2014).

[22] Y. Liu, T. Miller, and T.-C. Chiang, Appl. Phys. Lett. **95**, 243114 (2009).

[23] A. L. Walter, F. Schiller, M. Corso, L. R. Merte, F. Bertram, J. Lobo-Checa, M. Shipilin, J. Gustafson, E. Lundgren, A. X. Brión-Ríos, P. Cabrera-Sanfelix, D. Sánchez-Portal, and J. E. Ortega, Nat. Commun. **6**, 8903 (2015).

[24] G. Prévot, L. Barbier, and P. Steadman, Surf. Sci. **604**, 1265 (2010).

[25] E. Hahn, H. Schief, V. Marsico, A. Fricke, and K. Kern, Phys. Rev. Lett. **72**, 3378 (1994).

[26] T.-C. Chiang, Surf. Sci. Rep. **39**, 181 (2000).

[27] P. Moras, Y. Weisskopf, J.-N. Longchamp, M. Erbudak, P. Zhou, L. Ferrari, and C. Carbone, Phys. Rev. B **74**, 121405(R) (2006).

[28] A. Locatelli, L. Aballe, T. O. Menteş, M. Kiskinova, and E. Bauer, Surf. Interface Anal. **38**, 1554 (2006).

[29] T. O. Menteş, G. Zamborlini, A. Sala, and A. Locatelli, Beilstein J. Nanotechnol. **5**, 1873 (2014).

[30] E. Bauer, Surface Microscopy with Low Energy Electrons. Springer-Verlag, New York (2014).

[31] M. Salmerón, S. Ferrer, M. Jazzar, and G. A. Somorjai, Phys. Rev. B **28**, 6758 (1983).

[32] S. Smadici, D. Mocuta, and R. M. Osgood, Phys. Rev. B **69**, 035415 (2004).

[33] S. Smadici and R. M. Osgood, Phys. Rev. B **71**, 165424 (2005).

[34] P. Moras, D. Wortmann, G. Bihlmayer, L. Ferrari, G. Alejandro, P. H. Zhou, D. Topwal, P. M. Sheverdyaeva, S. Blügel, and C. Carbone, Phys. Rev. B **82**, 155427 (2010).

[35] J. F. Sánchez-Royo, J. Avila, V. Pérez-Dieste, M. De Seta, and M. C. Asensio, Phys. Rev. B **66**, 035401 (2002).

[36] T. Greber, T. J. Kreutz, and J. Osterwalder, Phys. Rev. Lett. **79**, 4465 (1997).

[37] R. Paniago, R. Matzdorf, G. Meister, and A. Goldmann, Surf. Sci. **336**, 113 (1995).

[38] K. Morgenstern, K.-F. Braun, and K.-H. Rieder, Phys. Rev. Lett. **89**, 226801 (2002).

[39] T. Uchihashi, P. Mishra, K. Kobayashi, and T. Nakayama, Phys. Rev. B **84**, 195466 (2011).

[40] N. Nagamura, I. Matsuda, N. Miyata, T. Hirahara, S.Hasegawa, and T. Uchihashi, Phys. Rev. Lett. **96**, 256801 (2006).

[41] N. Nagamura, R. Hobara, T. Uetake, T. Hirahara, M. Ogawa, T. Okuda, K. He, P. Moras, P. M. Sheverdyaeva, C. Carbone, K. Kobayashi, I. Matsuda, and S. Hasegawa, Phys. Rev. B **89**, 125415 (2014).

[42] P. Moras, W. Theis, L. Ferrari, S. Gardonio, J. Fujii, K. Horn, and C. Carbone, Phys. Rev. Lett. **96**, 156401 (2006).

[43] M. Henzler, Surf. Sci. **19**, 159 (1970).

[44] K. Besocke and H. Wagner, Surf. Sci. **52**, 653 (1975).

[45] N. C. Bartelt, T. L. Einstein, and E. D. Williams, Surf. Sci. **244**, 149 (1991).

[46] J. W. M. Frenken and P. Stoltze, Phys. Rev. Lett. **82**, 3500 (1999).

[47] R. C. Nelson, T. L. Einstein, and S.V. Khare, Surf. Sci. **295**, 462 (1993).

[48] M. Blanc, K. Kuhnke, V. Marsico, and K. Kern, Surf. Sci. **414**, L964 (1998).

Tables

	β_{Ag} (°)	Q_{Ag} (Å^{-1})	$\alpha_{Ag} + \beta_{Ag}$ (°)	α_{Ag} (°)	L_{Ag} (Å)	d_{Ag} (Å)
9 ML Ag film	2.42±0.25	0.223±0.015	7.05±0.40	4.63±0.40	28.1±1.6	28.2±1.6
15 ML Ag film	2.61±0.25	0.225±0.015	7.15±0.40	4.54±0.40	27.9±1.6	28.0±1.6
Model	1.97		6.73	4.76	28.33	28.35

Tabel I: Structural parameters of the Ag films on Pt(997) derived from the LEED analysis and from the model of Fig. 7(a).

Figures

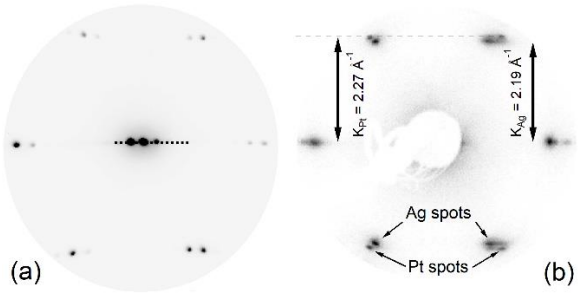

Figure 1: (a) Sum of micro-LEED images of clean Pt(997) taken every 1 eV in the range 20÷60 eV of primary energy with the SPELEEM instrument. (b) LEED image taken at 51.5 eV primary energy across the sharp edge between the clean Pt(997) surface and a 9 ML Ag film grown on it with the conventional LEED apparatus of the ARPES end-station (spot size ~1 mm diameter). The coexisting patterns allow to determine directly K_{Ag}.

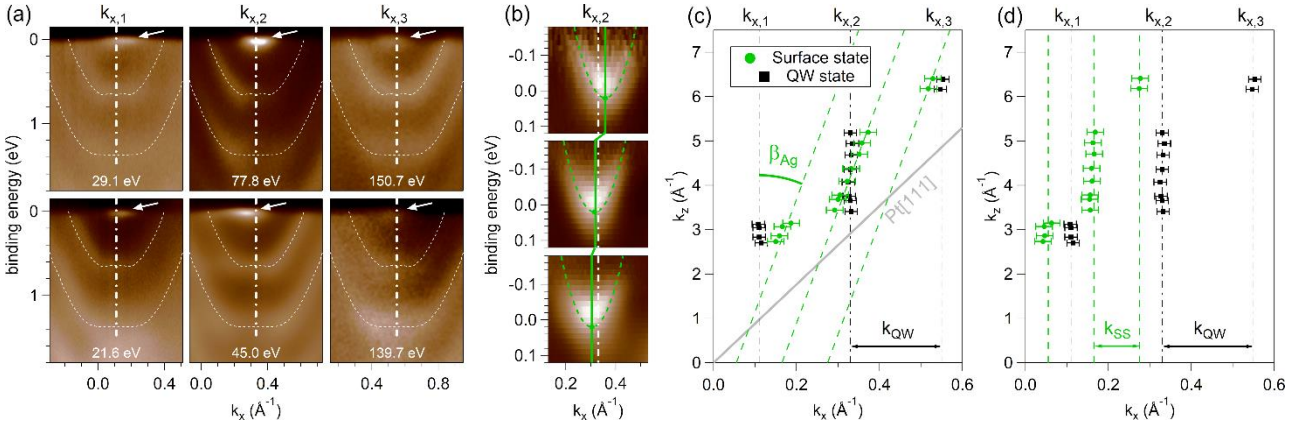

Figure 2: ARPES data for a 18 ML Ag film on Pt(997) along k_x. (a) Spectra at different photon energies (reported in the panels). Dashed lines mark the dispersion of the QW states. Arrows indicate the surface state. (b) Surface state band dispersion in the proximity of $k_{x,2}$ ($\hbar\omega$ = 47.9, 57.3, 87.2 eV from bottom to top). The green continuous line highlights the k_x shift of the surface state band center. (c) Structure plot showing the position of the band center for the surface and QW states. (d) Same as (c), upon applying the direct rotation correction to the surface state data.

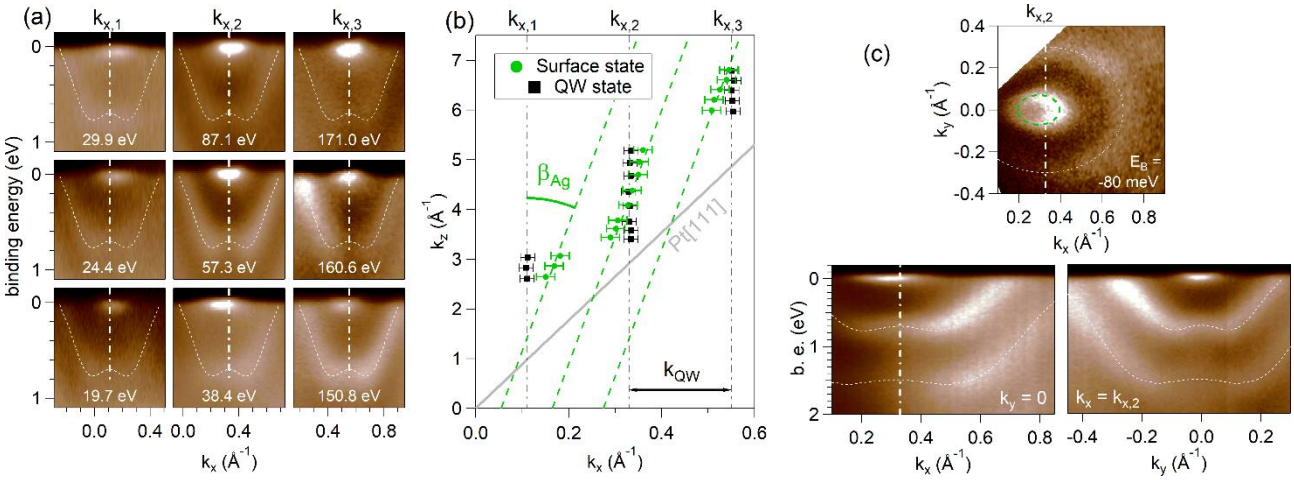

Figure 3: ARPES data for a 12 ML Ag film on Pt(997). (a) Spectra at different photon energies (reported in the panels). Dashed lines mark the dispersion of the QW state. (b) Structure plot showing the position of the band center for the surface and QW states. (c) Constant energy cut at 80 meV above E_F (top) and band dispersion along the k_x axis at $k_y = 0$ and along the k_y axis at $k_x = k_{x,2}$ (bottom). $\hbar\omega = 48.0$ eV.

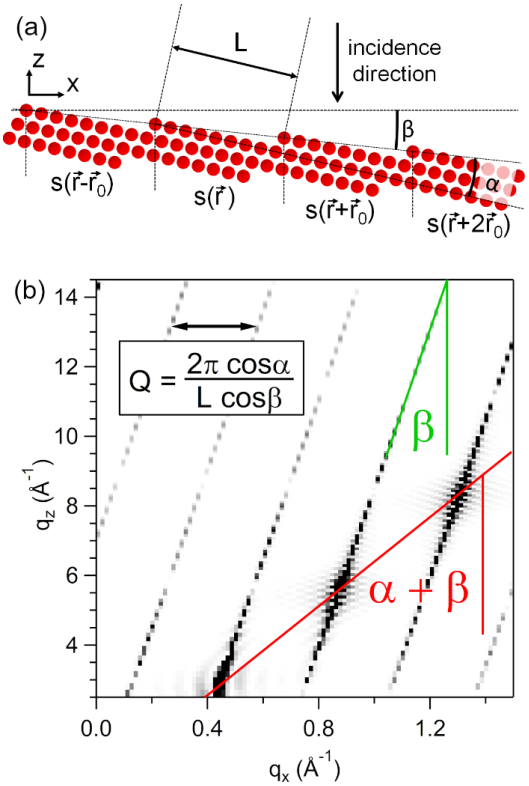

Figure 4: (a) Sketch of a stepped surface shown in profile view (step density corresponding to the Pt(997) surface). The incidence direction of the electron beam makes an arbitrary angle, β, with the average surface normal. (b) Kinematic simulation of the intensity of the specular beam in the q_x-q_z plane (the two axes have different scales). Red and green lines mark the angles α+β and β. The numerical values refer to the Pt(997) surface.

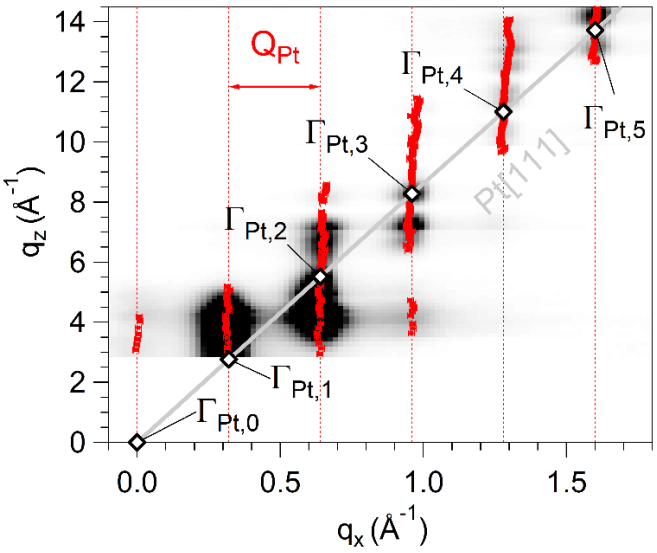

Figure 5: Intensity of the (0,0) LEED spot collected along the dotted line in Fig. 1(a). To compensate the strong intensity variations as a function of kinetic energy, the intensity is scaled differently in three regions of the image. Red dots highlight the position of the intensity maxima.

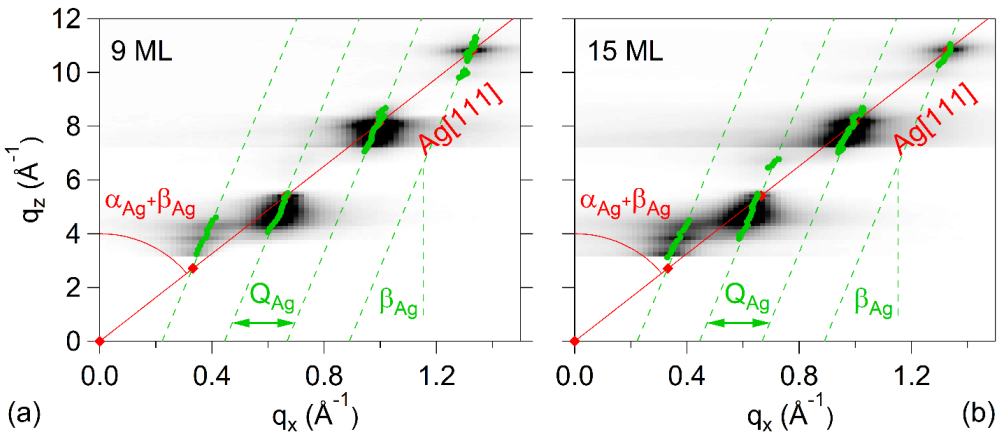

Figure 6: Intensity of the (0,0) LEED spot for (a) 9 ML and (b) 15 ML Ag films on Pt(997) in the q_x-q_z plane. The intensity is scaled differently in two regions of the images to compensate the strong intensity variations as a function of primary electron energy. Green dots mark the positions of the experimental maxima. The dashed lines indicate the inclination of the diffraction rods with respect to the q_z axis.

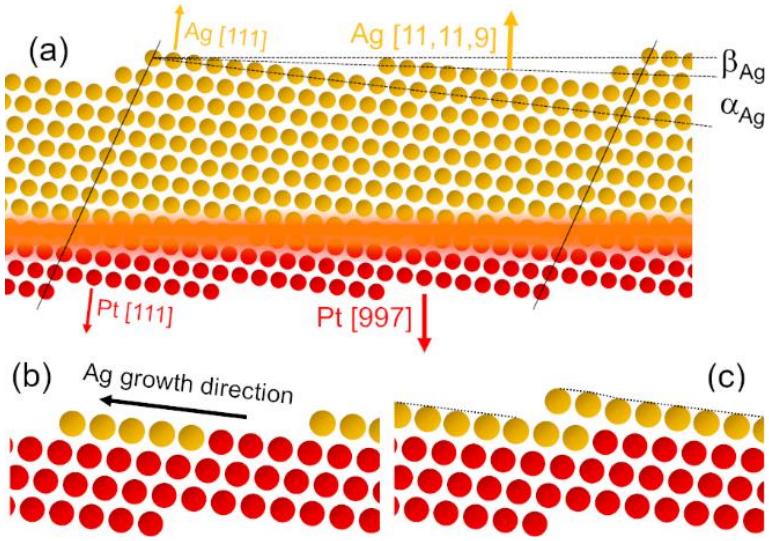

Figure 7: a) Side view of the structural model of a Ag film on Pt(997). Yellow and red spheres represent Ag and Pt atoms. The unknown interface morphology is hidden by a stripe oriented parallel to the Pt(997) plane. Small arrows indicate the orientation of the parallel Ag[111] and Pt[111] axes. Large arrows indicate the orientation of the Ag[11,11,9] and Pt[997] axes, which are separated by the β_{Ag} angle. b) Ag growth of 1D-like islands in contact with Pt(997). c) Initial growth of the second Ag layer.